Polaronic band tails in disordered solids: Combined effects of static randomness and electron-phonon interactions

C. H. Grein and Sajeev John

Department of Physics, Princeton University, P.O. Box 708, Princeton, New Jersey 08544

(Received 1 June 1987)

The band-tail density of states at zero temperature for an electron coupled to a quantized elastic continuum and static disorder is derived from first principles with use of a variational method based on the Feynman path-integral representation of the one-electron propagator. In the absence of static disorder, nonperturbative effects in the electron-phonon interaction associated with small-polaron formation give rise to an exponentially decaying band tail below the free-electron continuum. The density of states projected onto the phonon vacuum exhibits three physically distinct regimes when the electron-phonon coupling is above small-polaron threshold: (i) at shallow energies, there is a shift of the square-root continuum band edge arising from the perturbative emission and reabsorption of virtual phonons; (ii) at intermediate energies, there is a linear exponential band tail of localized states analogous to an Urbach tail arising from quantum fluctuations of the lattice; (iii) at deeper energies, there are strongly localized or self-trapped states associated with the termination of this band tail at the polaron ground state. In the infinite-effective-mass approximation for polaron formation, these results are in close agreement with a simple physical argument based on an optimum potential-well method. In the presence of weak static disorder and electron-phonon coupling near polaron threshold we find substantial synergetic interplay between phonons and disorder. Static potential fluctuations provide nucleation centers for small-polaron formation and an exponential tail appears for any value of the coupling constant. The resulting density of states can be considerably larger than that arising from static disorder and electron-phonon interaction acting individually.

I. INTRODUCTION

The electronic properties of disordered solids is a subject of fundamental importance in solid-state physics. The electronic structure of such materials results from an interplay between order and disorder giving rise to the phenomenon of band gaps or pseudogaps in the one-electron density of states (DOS). Associated with this behavior are the phenomena of band tailing and localization. These effects play a central role in determining both the optical and transport properties of the material. Theoretical efforts to describe band tailing[1-12] and localization[13-15] have been based largely on models in which an electron interacts with a static random potential arising from impurities in a doped semiconductor or structural disorder in the case of an amorphous semiconductor. However, it is well known that in the presence of a deformable medium which can respond to the motion of a conduction electron, self-trapping or polaronic effects may occur even in the absence of static disorder.[16-21] Associated with polaron formation is the density of excited states of the coupled electron-lattice system. Recently it was shown by one of us[22] that the projected density of states onto the zero-phonon sector of the lattice Hilbert space exhibits an exponentially decaying band tail of self-trapped states at zero temperature even in the absence of static disorder. This is analogous to an Urbach-Martienssen tail observed originally[23] in experiments on optically induced valence- to conduction-band electronic transitions in silver and alkali halides. It is the aim of this paper to extend the results of Ref. 22, which describes band tailing in an infinite-effective-mass approximation for the polaron, to include the effects of nonadiabaticity of the electron-phonon interaction. We consider also the combined effects of static disorder and electron-phonon interaction at zero temperature.

We find that for a large variety of electron-phonon coupling strengths, nonadiabaticity parameters, and static disorder potentials that the DOS, ρ_0, projected onto the phonon vacuum exhibits a linear exponential band tail throughout the energy range of experimental interest. Such a projected density of states is relevant to optical absorption experiments which take place on a time scale fast compared to the time required for lattice motion. In the deep tail, ρ_0 measures the overlap of the undistorted lattice wave function with that of the displaced lattice in the true polaron ground state. These results provide insight into the near universality of the Urbach tails in disordered materials. As in the case of band tails arising from static disorder alone,[7] the scale of the localized electronic wave function is comparable to the interatomic spacing in the solid throughout most of the experimentally relevant energy range. The effect of this correlation length in both the static and dynamic (phonon) components of the disorder is a broad crossover regime between a Halperin-Lax[3] band-tail DOS in which the wave function extends over many lattice spacings and a deep-tail Gaussian DOS in which the wave function is localized on the scale of 1 Å. The effective-mass approximation for an electron near the conduction-band edge remains valid throughout most of the Urbach tail which in some materials may extend nearly one-quarter of the way into the band gap. Real band-structure effects such as the presence of the valence

band, in general, render the deep Gaussian tail inaccessible in actual materials.

In the case of relatively weak static disorder, the effect of electron-phonon interactions is more pronounced. Static potential fluctuations provide nucleation centers for small-polaron formation. The result is a synergetic interplay between static localization and polaron formation. This leads to a substantial increase in the band-tail density of states even for electron-phonon coupling below small-polaron threshold.

The technique used in the calculation of the electron propagator is the path-integral method introduced by Feynman[17] to calculate the polaron ground-state energy. The effects of disorder and electron-phonon interaction are simulated by means of a harmonic trial action in which the electron is coupled to a fictitious mass M_{trial} with a spring constant K_{trial} and first-cumulant expansion of the true action about this trial action is performed. The density of states at any given energy E is obtained by optimizing the parameters M_{trial} and K_{trial} according to a variational technique. These results are compared to a simple physical argument based on maximizing the probability of occurrence of a static potential well supporting a bound state at precisely the energy E. We find that this physical argument gives results in quantitative agreement with the path-integral method in the static ($M_{trial} = \infty$) limit. By allowing M_{trial} to be a finite variational parameter, the nonadiabaticity of the electron-phonon interaction is taken into account. This leads to an increase in the overall density of states as well as the appearance of a shifted continuum-band edge associated with the emission and reabsorption of virtual phonons in the disordered medium. In the vicinity of the shifted band edge there are two solutions of the variational problem, one corresponding to a nearly free electron for which $M_{trial} \ll m$, the free-electron band mass, and one corresponding to a small polaron for which $M_{trial} \gg m$. Quantum mechanically these two states are connected by means of a nonzero tunneling amplitude determined by the nonadiabaticity of the electron-phonon interaction. A detailed treatment of this tunneling effect, however, requires the use of a more general trial action than we have considered here.

In Sec. II we review the behavior of the polaron ground-state energy as a function of the electron-phonon coupling strength and nonadiabaticity in the absence of static disorder. In Sec. III the associated band-tail density of states is derived by means of a simple physical argument and comparison is made with the path-integral method. In Sec. IV we consider the combined effects of static disorder and coupling to phonons in the band tail. A derivation of the variational principle used in the path-integral method is given in the Appendix.

II. THE POLARON GROUND STATE

Consider the interaction between an electron and acoustic phonons in a crystal. The Hamiltonian for this system is[19]

$$H = H_e + H_{ac} + H_{e\text{-}ac} ,$$ (2.1a)

where

$$H_e = p^2/2m$$ (2.1b)

is the kinetic energy of an electron of band mass m,

$$H_{ac} = \frac{M}{2} \sum_k (|\dot{q}_k|^2 + w_k^2 |q_k|^2)$$ (2.1c)

is the harmonic phonon energy for a lattice of atoms of mass M, and

$$H_{e\text{-}ac} = \frac{E_d}{u} \sum_k \dot{q}_k \frac{e^{i\mathbf{k}\cdot\mathbf{x}}}{\sqrt{N}}$$ (2.1d)

is the deformation-potential interaction. We consider for simplicity a cubic crystal at zero temperature containing N atoms. The wave-vector summation extends over all points in the first Brillouin zone. The normal coordinate of a longitudinal acoustic phonon of wave vector $\mathbf{k}$ and frequency $w_k \equiv uk$ is $q_k \equiv \hat{\mathbf{k}} \cdot \mathbf{q}_k$, where u is the speed of sound. It is related to the lattice displacement field $\mathbf{u}$ through

$$\mathbf{u}(\mathbf{x}) = \sum_k \mathbf{q}_k \frac{e^{i\mathbf{k}\cdot\mathbf{x}}}{\sqrt{N}} .$$ (2.2)

E_d is the deformation-potential energy constant and following Sumi and Toyozawa we define a dimensionless acoustic coupling constant S_{ac} through the relation $\hbar u k_0 S_{ac} \equiv E_d^2/2Mu^2$, where $k_0 = \pi/a_0$ and a_0 is the lattice spacing.

This model has been studied by Sumi and Toyozawa,[19] who obtained the ground-state energy of this system in the strong-coupling limit. They found that as the coupling constant increases, the acoustic polaron undergoes a discontinuous transition from the nearly free type to the self-trapped type, where these two polaron states are separated by a nucleation barrier.

The ground-state energy is a function of two physical parameters: the nonadiabaticity parameter $\gamma = \hbar u k_0 / \varepsilon_B$, measuring the ratio of the speed of sound u to the speed of an electron at wave number k_0, where $\varepsilon_B = \hbar^2 k_0^2/2m$, and the electron–acoustic-phonon coupling constant S_{ac}. A continuum version of this model may be obtained by replacing the wave-vector sum by a weighted integral

$$\sum_k \rightarrow \frac{V}{(2\pi)^3} \int d^3k \, H_C(k) .$$ (2.3a)

Here V is the volume of the solid.

John and Cohen[21] considered a cubic Brillouin zone with sides of length $2\pi/a_0$ with a soft cutoff on the wave vectors:

$$H_C(k) = \exp\left[-\frac{\pi}{4} \left[\frac{k}{k_0} \right]^2 \right] .$$ (2.3b)

This choice of a cutoff function preserves the volume of the Brillouin zone of this simple cubic crystal. They showed that the polaron ground-state energy could be expressed analytically in terms of two variational parameters R and λ. R is the dimensionless radius of the polaron measured in units of k_0^{-1} and can be defined precise-

ly in terms of the variational parameters K_{trial} and M_{trial} entering the trial harmonic oscillator action described in the previous section. Introducing the reduced mass $\mu \equiv m M_{trial}/(m + M_{trial})$ and the frequency $\nu \equiv (K_{trial}/\mu)^{1/2}$, the polaron radius is $R \equiv k_0^{-1}\sqrt{\hbar/\mu\nu}$. Introducing the total mass $m_T \equiv M_{trial} + m$, we define a second parameter $\lambda \equiv (m/m_T)^{1/2}$. The scaling form of the ground-state energy measured in units of the Debye energy $\hbar u k_0$ is then given by

$$E_G(R,\lambda) = \frac{3}{2\gamma R^2}\left[\frac{1-\lambda}{1+\lambda}\right] - \frac{\pi}{2}S_{ac}\left[\frac{\gamma}{\lambda^2}\right]^3 F(\alpha) ,$$

$$0 < \lambda < 1, \quad 0 < R < \infty \quad (2.4a)$$

where

$$F(\alpha) = \int_0^\infty dq \frac{q^2}{1+q}e^{-\alpha q^2} \quad (2.4b)$$

and

$$\alpha = \frac{1}{2}\left[\frac{\gamma}{\lambda^2}\right]^2 [\pi + R^2(1-\lambda^2)^2] . \quad (2.4c)$$

The two parameters R and λ are independent variational parameters which are chosen to minimize $E_G(R,\lambda)$. Here λ measures the extent of nonadiabaticity, and in the limit $\lambda \to 0$, (2.4a) reduces to the Emin-Holstein[20] scaling expression for the polaron ground-state energy.

For small γ, E_G has two local minima with respect to the variational parameters over a wide range of values of S_{ac}. These minima correspond to the nearly free electron and the small (self-trapped) polaron. The small-polaron local minimum E_{GS} becomes more stable when the sum of the electron-phonon interaction energy, the lattice distortion energy, and the electron kinetic energy due to localization becomes more negative than the energy E_{GL} of a nearly free electron with a perturbative self-energy shift. The zero of the energy has been chosen to be that of a completely decoupled electron at rest in the phonon vacuum.

The values of λ and R which minimize E_G are determined numerically. Figures 1(a)–1(c) present the polaron ground-state energy, radius, and effective mass for choice of a cubic Brillouin zone and cutoff function (2.3b). The results are qualitatively the same as those of Sumi and Toyozawa, the quantitative differences being due to different choices for Brillouin zone shape and wave-vector cutoffs.

The threshold for small-polaron formation occurs when $E_{GS} = E_{GL}$. It depends weakly on γ: as γ goes from 0.1 to 0.01, the threshold varies from $S_{ac}\gamma \approx 5.1$ to 3.7. In the static approximation $(\lambda=0)$,

$$E_G(R) = \frac{3}{2\gamma R^2} - \frac{S_{ac}}{2^{3/2}}\frac{1}{(1+R^2/\pi)^{3/2}} \quad (2.5)$$

and the threshold for small-polaron formation is slightly lower: $S_{ac}\gamma \approx 3.5$. Thus the incorporation of nonadiabaticity $(\lambda>0)$ leads to higher threshold for small-polaron formation due to the existence of a competing large-polaron state.
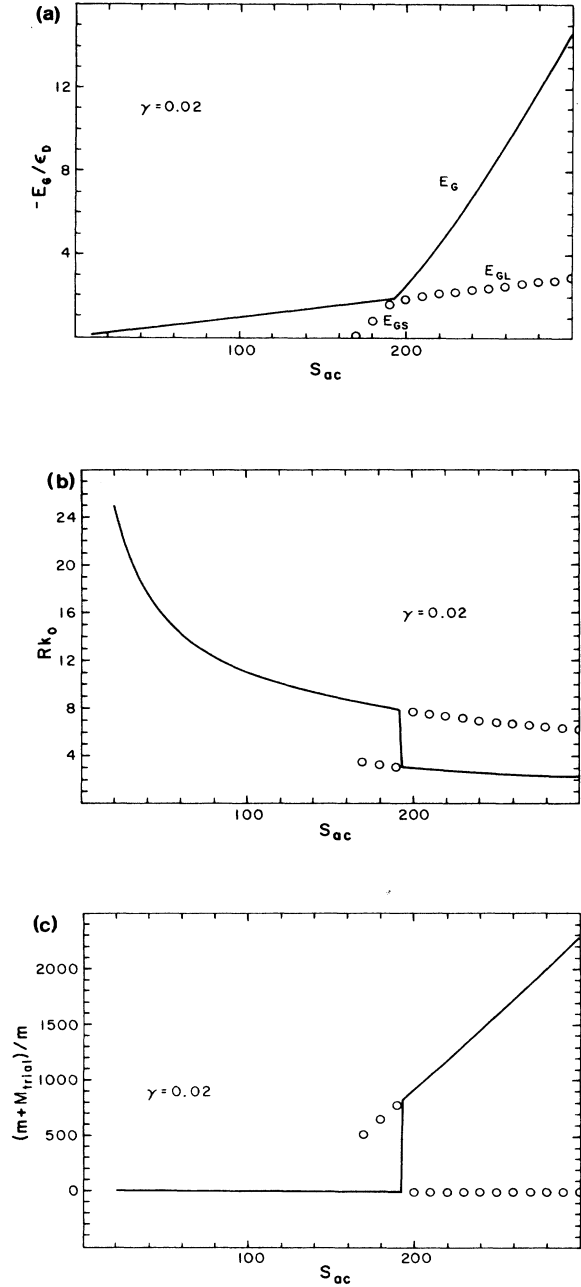
In summary, nonadiabaticity $(\lambda>0)$ results in both

FIG. 1. (a) Acoustic-polaron ground-state energy as a function of the electron-phonon coupling constant. For $S_{ac} \leq 192$, the nearly-free-electron state has a lower energy E_{GL} than the small polaron. For $S_{ac} \geq 192$, the small-polaron E_{GS} has the lower energy. The solid line E_G depicts the energy of the lower-energy solution and the dotted line gives the higher-energy solution. The small-polaron solution does not exist for coupling less than $S_{ac} \approx 168$. (b) Polaron radius as a function of S_{ac}. The Debye wave vector is defined as $k_0 \equiv \pi/a_0$, where a_0 is the lattice spacing. The small-polaron radius is approximately equal to the lattice spacing whereas the nearly-free-electron state radius is many times greater than the lattice spacing. (c) Polaron effective mass as a function of S_{ac}. Here, m is the electron band mass. For the nearly free electron, M_{trial} is of the order of $10^{-5}m$.

the static small-polaron and free-electron solutions of (2.5) becoming unstable with respect to the lower-energy, finite-effective-mass polaron solutions of (2.4a). The small-polaron solution is characterized by small positive λ and R of the order of the lattice spacing, whereas the nearly-free-electron solution has λ slightly less than 1 and R much larger than the lattice spacing. In the trial action method introduced by Feynman, the switching of the ground-state E_G from the nearly-free-electron minimum E_{GL} to the small-polaron local minimum E_{GS} at a critical value of the coupling constant S_{ac} appears at a kink in the ground-state energy. It also leads to a discontinuity in the polaron radius and polaron effective mass. This singularity, however, is an artifact of the trial action method. Quantum mechanically, there is a tunneling amplitude between the two solutions and the true ground state is a superposition of the two. The tunneling amplitude is proportional to the overlap of the electronic and lattice wave functions between the two states. In the static limit $(M_{trial} = \infty)$ the electronic wave function in the small-polaron state is strongly localized whereas the free-electron wave function is extended and has a normalizing factor proportional to $1/\sqrt{V}$, where V is the volume of the crystal. It follows that in the thermodynamic limit $V \rightarrow \infty$, the overlap between the two states vanishes. If, on the other hand M_{trial} is finite, then the small polaron is free to move and a nonzero tunneling amplitude between the self-trapped and extended state exists. It is likely that a more general trial action would be required to describe this effect.

III. DENSITY OF STATES FOR AN ELECTRON IN A QUANTUM FIELD

Associated with the small-polaron ground state described in Sec. II is the density of excited states of the coupled electron-phonon system. Previously,[22] the projected density of states onto the phonon vacuum was obtained in the static $(M_{trial} = \infty)$ approximation by means of the Feynman path integral. In this section we demonstrate explicitly that this result for the exponential band tail of a coupled electron-phonon system in the absence of static disorder may be recaptured by means of a simple physical argument. The calculation is then generalized to the nonadiabatic case by means of the path integral.

Consider the quantum-mechanical probability distribution for normal coordinates q_k of the lattice at zero temperature:

$$P\{q_k\} \propto \exp\left[-\sum_k \frac{M\omega_k}{\hbar} |q_k|^2 \right] .$$ (3.1)

This is the probability distribution for the lattice in its unperturbed ground state and is obtained by taking the product over all $\mathbf{k}$ in the Brillouin zone of the ground-state wave function of the normal coordinate q_k:

$$\psi_0(q_k) = (M\omega_k/\pi\hbar)^{1/4} \exp[-(M\omega_k/2\hbar) |q_k|^2] .$$ (3.2)

We consider a lattice fluctuation of the form

$$q_k = \frac{iQ_0}{\sqrt{N}} \exp\left[-\frac{k^2 b^2}{4} \right]$$ (3.3)

of depth Q_0 and range b. In order to make contact with the continuum theory it is convenient to replace the wave-vector summation in (3.1) by an integral:

$$\sum_k \rightarrow \frac{V}{(2\pi)^3} \int d^3k \, C^{-1}(k)$$ (3.4a)

with autocorrelation function $C(k)$ chosen to have a Gaussian form, with correlation length $\sqrt{2\pi}/k_0$:

$$C(k) = \exp\left[-\frac{\pi k^2}{2k_0^2} \right] .$$ (3.4b)

Since it is the cutoff on the wave-vector summation which determines the spatial correlation of the lattice fluctuations, the autocorrelation function is the Brillouin-zone cutoff function (2.3b) squared.

The probability of occurrence of a fluctuation of the form (3.3) is given by

$$P\{q_k\} \propto \exp\left[-\left[\frac{\pi}{bk_0} \right]^4 \frac{\hbar u k_0}{2\pi^3(\hbar^2/2MQ_0^2)} \right.$$
$$\left. \times \left[1 - \frac{\pi}{(bk_0)^2} \right]^{-2} \right] .$$ (3.5)

Such a potential fluctuation contributes to the DOS at a particular energy $-|E|$ provided the ground-state binding energy of an electron in this well plus the elastic distortion energy of the well equal $-|E|$. This places a constraint on the variational parameters Q_0 and b expressed by the radial Schrödinger equation

$$\left[-\frac{\hbar^2}{2m} \frac{d^2}{dr^2} + \frac{E_d}{u} \sum_k \dot{q}_k \frac{e^{i\mathbf{k}\cdot\mathbf{r}}}{\sqrt{N}} \right.$$
$$\left. + \frac{M}{2} \sum_k \omega_k^2 |q_k|^2 \right] u(r) = -|E| u(r) ,$$ (3.6)

where $u(r) \equiv r\psi(r)$. Equation (3.6) contains two potential terms: the deformation potential describing interaction between the electron and acoustic phonons, and the lattice distortion energy.

Probability distribution (3.5) is maximized with respect to the variational parameters subject to the constraint (3.6). The function $u(r)$ is given the boundary conditions $u(0) = u(\infty) = 0$ and the radius coordinate in the radial Schrödinger equation is discretized. Then (3.6) becomes a matrix eigenvalue equation which can be solved for one variational parameter given the other. The numerical solution method used here chose successive values of b, each time solving the Schrödinger equation for Q_0, and calculated (3.5) until the value of b was found which maximized (3.5). The density of states $\rho_0(E)$ projected onto the phonon vacuum is then proportional to the probability distribution (3.5) with Q_0 and b chosen in this manner for every value of the energy. This procedure gives the exponential part of the DOS provided that the potential fluctuations oscillate on time scales long compared with the time needed for the elec-

tron to localize. Consider an electron harmonically bound to a lattice deformation with a harmonic oscillator frequency v. The radius of the lattice deformation is then $R \approx \sqrt{\hbar/mv}$. The oscillation frequency of this potential well is dominated by the frequency of the associated phonon of wavelength R: $\omega_R \equiv 2\pi u(mv/\hbar)^{1/2}$. Thus in the very shallow tail, where the electron is weakly bound, $v < \omega_R$ as $v \to 0$ so the potential wells may begin to oscillate on time scales shorter than the time needed for the electron to localize. Numerically, we find that except when the electron-phonon coupling is very strong $v > \omega_R$ for all energies below zero.

Figure 4 depicts the DOS obtained by this method and compares it with the predictions of the methods discussed next. Here, the electron oscillation frequency is greater than the well oscillation frequency for all energies less than zero. The physical argument does not restrict the wave function to a particular form whereas the variational method based on the path integral discussed next involves the restriction of the wave function to a harmonic oscillator form. Thus the DOS obtained from the physical argument is slightly greater for all energies than that predicted by the variational method in the static ($M_{\text{trial}} = \infty$) limit.

A more general formulation which goes beyond the static approximation follows from the one-electron Green's function for an electron interacting with acoustic phonons. This may be represented using the Feynman path integral. Previously, John[22] defined a projected DOS using the matrix element of the time evolution operator

$$G_0(\mathbf{x},0 \mid \mathbf{x},t) \equiv \langle \psi_0; \mathbf{x} \mid \exp(-iHt/\hbar) \mid \psi_0; \mathbf{x} \rangle , \qquad (3.7)$$

where $\mathbf{x}$ is the electron coordinate and ψ_0 is the ground-state wave function of the unperturbed lattice. This matrix element has the Feynman path-integral representation

$$G_0(0,0 \mid 0,t) = \int D\mathbf{x}(\tau) e^{iS_{\text{eff}}/\hbar}, \quad \mathbf{x}(0) = \mathbf{x}(t) = 0 \qquad (3.8)$$

where the effective action S_{eff} is obtained from the true action by integration over all phonon coordinates. S_{eff} has the form

$$S_{\text{eff}} = \frac{m}{2} \int_0^t d\tau\, \dot{\mathbf{x}}^2(\tau)$$

$$+ \int_0^t d\tau \int_0^t d\tau' \frac{1}{N} \sum_{\mathbf{k}} e^{-i\mathbf{k}\cdot[\mathbf{x}(\tau)-\mathbf{x}(\tau')]}$$

$$\times \frac{\hbar u k_0}{2} S_{\text{ac}} i\omega_k e^{-i\omega_k |\tau-\tau'|} . \qquad (3.9)$$

As described previously,[21] the continuum limit used in Sec. II is obtained by replacing the wave-vector summation by an integral with cutoff function $H_C^2(k)$ given by (2.3b). The diagonal component of the Green's function is independent of $\mathbf{x}$ due to translational symmetry. The DOS projected onto the phonon vacuum follows from

$$\rho_0(E) = \int_{-\infty}^{\infty} \frac{dt}{2\pi\hbar} e^{iEt/\hbar} G_0(0,0 \mid 0,t) . \qquad (3.10)$$

Such a projection is relevant to optical absorption events which occur on time scales short compared with the time scales for lattice distortions needed for true self-trapping.[22]

The Green's function is approximated by a first-cumulant expansion about a trial action[21,24] which describes an electron coupled to a trial mass M_{trial} through a spring with spring constant K_{trial}. Both K_{trial} and M_{trial} are variational parameters. The trial action is

$$S_{\text{trial}} = \frac{m}{2} \int_0^t d\tau\, \dot{\mathbf{x}}^2(\tau)$$

$$- \frac{a}{2} \int_0^t d\tau \int_0^t d\tau' \mid \mathbf{x}(\tau) - \mathbf{x}(\tau') \mid^2$$

$$\times \frac{\cos[b(\mid \tau-\tau' \mid -t/2)]}{\sin(bt/2)}$$

$$(3.11)$$

and

$$K_{\text{trial}} = \frac{4a}{b}, \quad M_{\text{trial}} = \frac{4a}{b^3} . \qquad (3.12)$$

Here, the position of the mass M_{trial} has been eliminated by performing a trace over its coordinate.

The first-cumulant approximation to the Green's function is

$$\int D\mathbf{x}(\tau) e^{iS_{\text{eff}}/\hbar} \approx J_{\text{trial}} e^{i\langle S_{\text{eff}} - S_{\text{trial}} \rangle/\hbar} , \qquad (3.13)$$

where[24]

$$J_{\text{trial}} = \int D\mathbf{x}(\tau) e^{iS_{\text{trial}}/\hbar}$$

$$= \left[\frac{m}{2\pi i\hbar t} \right]^{3/2} \left[\frac{v \sin(bt/2)}{b \sin(vt/2)} \right]^3 \qquad (3.14)$$

and the angular brackets denote averaging with respect to S_{trial}:

$$\langle A \rangle \equiv \frac{\int D\mathbf{x}(\tau)\, A e^{iS_{\text{trial}}/\hbar}}{\int D\mathbf{x}(\tau) e^{iS_{\text{trial}}/\hbar}} . \qquad (3.15)$$

It has been shown that[21,24]

$$\frac{i}{\hbar} \langle S_{\text{eff}} - S_{\text{trial}} \rangle = I_0(t) + I_{\text{int}}(t) , \qquad (3.16a)$$

where

$$I_0(t) = \frac{3\mu}{2m} \left[\frac{vt}{2} \cot\left[\frac{vt}{2} \right] - 1 \right] , \tag{3.16b}$$

$$I_{\text{int}}(t) = -\frac{\pi}{2} S_{\text{ac}} \left[\frac{u}{k_0} \right]^2 \int_0^t d\Delta(t-\Delta) \int_0^\infty dk\, k^3 \exp\left[-\frac{k^2}{2k_0^2}[\pi - iQ(\Delta;t)] - iuk\Delta \right] \tag{3.16c}$$

and

$$Q(\Delta;t) = \hbar k_0^2 \left[\frac{2\mu}{m^2 v} \frac{\sin(v\Delta/2)\sin[v(\Delta-t)/2]}{\sin(vt/2)} + \frac{(\Delta-t)\Delta}{(m+M_{\text{trial}})t} \right] . \tag{3.16d}$$

It follows from (3.14) that the approximate Green's function has poles along the real time axis spaced by $2\pi/v$, the period of oscillation of the trial harmonic oscillator. It is convenient to shift the time contour in (3.10) into the lower half complex time plane and perform the integration over all real t', where $t = -iT + t'$ (Fig. 2).

For imaginary time $t = -iT$, and with the choice $vT \gg 1$, Eqs. (3.16b) and (3.16d) may be approximated by

$$I_0(t) \approx \frac{3\mu}{4m} vit - \frac{3\mu}{2m} , \tag{3.17a}$$

$$Q(\Delta;t) \approx i\hbar k_0^2 \left[\frac{\mu}{m^2 v} - \frac{i(\Delta-t)\Delta}{tm_T} \right] , \tag{3.17b}$$

so

$$e^{iEt/\hbar} G_0(0,0 \mid 0,t) \approx \left[\frac{m_T}{2\pi i \hbar t} \right]^{3/2} \sin^3\left[\frac{bt}{2} \right] \exp[F(t)] , \tag{3.18}$$

where

$$F(t) = -\frac{3\mu}{2m} + it\left[\frac{E}{\hbar} + \frac{3\mu v}{4m} - \frac{3v}{2} \right] + I_{\text{int}}(t) \tag{3.19a}$$

and

$$I_{\text{int}}(t) = -\frac{\pi}{2} S_{\text{ac}} \int_0^{\omega_0 t} d\Delta\,(\omega_0 t - \Delta) \int_0^\infty dq\, q^3 \exp\left[-\frac{q^2}{2}[\pi - iQ(\Delta;t)] - iq\Delta \right] . \tag{3.19b}$$

Here $\omega_0 \equiv uk_0$ is the Debye frequency.

The second term of the kernel Q allows for the motion of the center of mass of the polaron with total mass $m + M_{\text{trial}}$ through the medium. The function $F(t)$ has a saddle point along the negative imaginary time axis at $t_s = -iT_s$ for energies above the polaron ground-state energy. If T_s is small compared to the time needed for the center of mass to move a lattice spacing then the second term of Q can be neglected. This is the infinite-effective-mass approximation $(M_{\text{trial}} = \infty)$. Later the effects of a finite effective mass will be discussed.

In a saddle-point approximation the DOS becomes

$$\rho_0(E) \approx \frac{1}{2\pi\hbar} \left[\frac{mv^2 T_s}{2\pi\hbar} \right]^{3/2} \left[\frac{2\pi}{|F''(t_s)|} \right]^{1/2} \exp[F(t_s)] , \tag{3.20}$$

which is valid as long as the next term in the expansion of $F(t)$ about t_s is small:

$$\frac{F^{(4)}(t_s)}{8|F''(t_s)|^2} = \frac{5}{6\pi} \frac{(\omega_0 T_s)^2}{S_{\text{ac}}} \ll 1 , \tag{3.21}$$

where $F^{(4)}(t_s)$ denotes the fourth derivative of $F(t_s)$ with respect to t_s. The time at the saddle point is given by the saddle-point equation
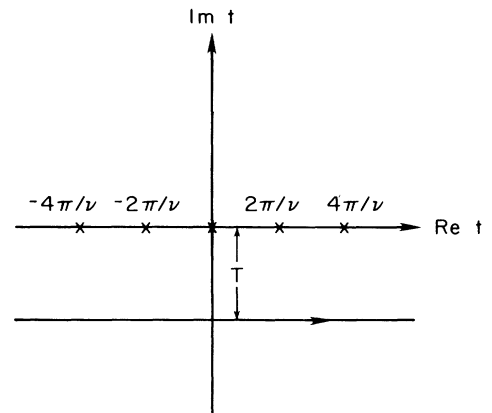

FIG. 2. The integrand of the time integral to obtain the DOS has poles spaced by $2\pi/v$ along the real time axis, thus the time integral is interpreted as a contour integral in the lower half complex time plane. The contour crosses the imaginary time axis at $t = -iT$.

$$F'(t_s)=0 \Rightarrow E-E_G(\nu)=\frac{\pi\hbar\omega_0 S_{ac}}{2(\pi/2+\varepsilon_B/\hbar\nu)^{3/2}}I_2(\beta) ,$$

$$(3.22)$$

where

$$E_G(\nu)=\frac{3\hbar\nu}{4}-\frac{\gamma S_{ac}\varepsilon_B}{2^{3/2}\left[1+2\varepsilon_B/\pi\hbar\nu\right]^{3/2}}$$

$$(3.23)$$

is the scaling form of the static polaron ground-state energy [equivalent to (2.5)]. The parabolic cylinder function with argument $\beta=iuk_0t(\pi/2+\varepsilon_B/\hbar\nu)^{-1/2}$ is

$$I_n(\beta)=\int_0^\infty dq\, q^n \exp(-q^2-\beta q) .$$

$$(3.24)$$

The exponential part of the DOS becomes

$$F(t_s)\approx(\omega_0 T_s)\frac{E-E_G(\nu)}{\hbar\omega_0}-\frac{\pi}{2}S_{ac}\frac{I_1(0)-I_1(\beta)}{(\pi/2+\varepsilon_B/\hbar\nu)} .$$

$$(3.25)$$

In the limit of small time at the saddle point ($\beta \ll 1$), the DOS behaves as[22]

$$\rho_0(E)\sim\exp\left[\frac{-21.1|E|}{S_{ac}\gamma^2\varepsilon_B}\right]$$

$$(3.26)$$

over energy ranges where the small-time approximation is valid. However, the small-time approximation fails in the deep and shallow tail regions. In the shallow tail, the small-time approximation loses self-consistency as the time scale of oscillations of the potential wells becomes comparable to the time of oscillation of the electron in the well. In the deep tail, the electron must dig its own potential well rather than stabilizing one that already exists, resulting in the saddle point T_s diverging as the energy approaches the polaron ground-state energy. Thus a numerical solution is now obtained without making any assumptions about the magnitude of the time at the saddle point. As shown in the Appendix, the greatest lower bound to the true DOS is obtained by maximizing the exponential part of the DOS in the saddle-point approximation with respect to the variational parameters. For infinite trial mass, the numerical solution method considers ν to be a function of T_s, the time at the saddle point. For a given choice of ν, T_s is found by minimizing the exponential part of the DOS with respect to T_s and this is repeated for successive choices of ν until that value is found which maximizes the exponential part of the DOS.

Figure 3 depicts the band tail DOS for the choice $\gamma=0.01$, $M_{trial}=\infty$, and several values of S_{ac}. As γ approaches zero, the small-time approximation improves so the DOS approaches its analytic (small-time) values (3.26) in the Urbach regime. The density of states at zero energy is a measure of the probability of a potential fluctuation which results in the total energy being zero, where the total energy is the sum of the electron kinetic energy, the deformation-potential energy and the lattice distortion energy.

As discussed in the previous section, the threshold for small polaron formation is given by $S_{ac}\approx3.5$ in the
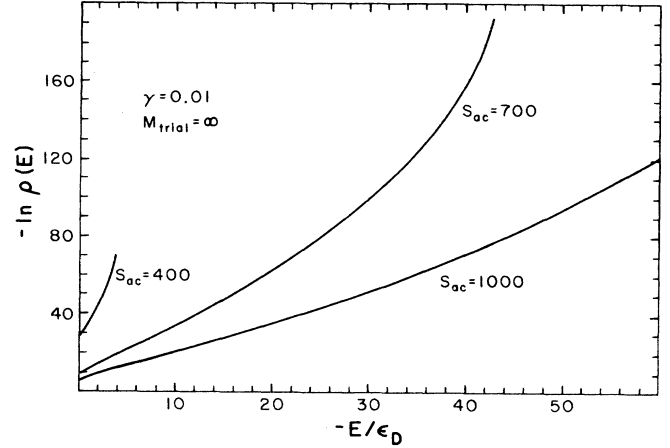

FIG. 3. Band-tail DOS for an electron in a quantum field with no static disorder. In the infinite-effective-mass approximation, the DOS is depicted for three different coupling strengths $S_{ac}=400$, 700, and 1000. The corresponding small-polaron ground-state energies are $E_{GS}/\varepsilon_D\approx-3.9$, -43.4, and -97.0, where ε_D is the Debye energy. The DOS time contour integral is evaluated in the saddle-point approximation.

infinite-effective-mass approximation. The parameter γ is of the order of 10^{-2} in materials with band widths of the order of 1 eV.[19] Figure 3 presents three strong coupling cases beginning with $S_{ac}\gamma$ just above threshold. As $S_{ac}\gamma$ approaches threshold, the intermediate Urbach regime is pinched out but this can be prevented by including interaction with static disorder, as discussed in the next section.

The previous results for the DOS in the saddle-point approximation are now generalized by allowing M_{trial} to also be a variational parameter thus taking into account the nonadiabaticity of the electron-phonon interaction. For energies below E_{GL}, the nearly-free-electron solution of (2.4a), there exists a unique solution for the two variational parameters. However, at energies above E_{GL} but still below zero two different solutions are found, one corresponding to a nearly free electron ($M_{trial}\ll m$) and the other to a small polaron ($M_{trial}\gg m$). The small-polaron solution gives rise to a continuous DOS for $0>E>E_{GS}$; however, a second solution appears for $0>E>E_{GL}$ corresponding to the nearly free electron. The DOS for the latter solution is greater than for the former for energies $E>E_{GL}$ but becomes vanishingly small for $E_{GL}>E$. Quantum mechanically, there is a nonzero tunneling amplitude between the two solutions which the above trial action and saddle-point approximation do not take into account.

To improve the treatment of tunneling the time contour integral (3.10) is now evaluated explicitly rather than in the saddle-point approximation. Integration is done over all real t', where $t=-iT+t'$ (Fig. 2), and T is chosen to pass through a saddle point. The two variational parameters are chosen to maximize $\ln\rho_0(E)$. Figure 4(a) includes the band-tail DOS for $S_{ac}=700$, $\gamma=0.01$ where the entire contour integral is done. The DOS is continuous everywhere and exhibits only a single

solution for the variational parameters at all energies. The oscillation frequency of the electron, ν, is greater than the well oscillation frequency[22] $\omega_R \approx 2\pi u / R$ over the energy range depicted in Fig. 4(a); thus the potential wells oscillate on time scales longer than the time required for the electron to localize. This validates the as-
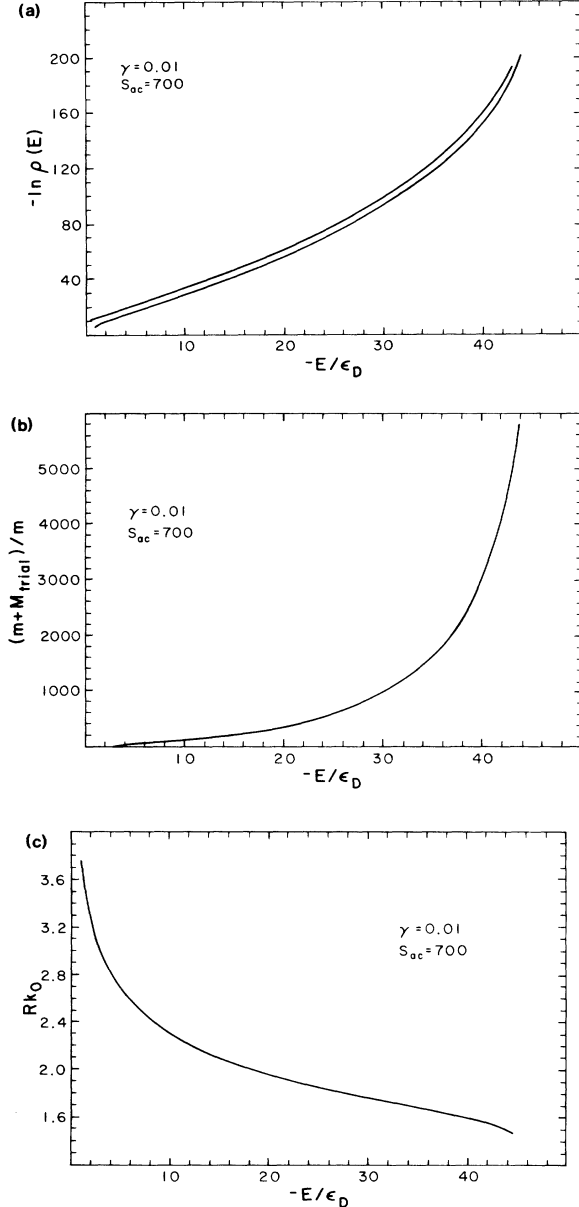

(a)

(b)

(c)

FIG. 4. (a) Band-tail DOS for an electron in a quantum field with no static disorder. The top curve is obtained from the path-integral method in the infinite-effective-mass approximation, and is indistinguishable from the prediction of the physical argument. The bottom curve is obtained from the path-integral method, with the trial mass of the trial action treated as a variational parameter. For the latter curve the DOS time contour integral is evaluated entirely. The small-polaron ground-state energy is $E_{GS}/\varepsilon_D \approx -44.1$ when the trial mass is allowed to be a variational parameter. (b) Polaron effective mass in the band tail. (c) Polaron radius in the band tail.

sumption of static potential wells. At zero energy, the logarithm of the DOS extrapolates to a value close to zero in contrast with the result $\ln\rho_0(0) = -9.7$ obtained in the finite effective-mass approximation. This is a consequence of the increase of the shallow-tail DOS due to a downshift of the continuum band edge. Figure 4(b) is a plot of the polaron effective mass in the band tail. The trial mass M_{trial} takes on a value intermediate between its values for the small polaron and nearly-free-electron states at energies greater than E_{GL}, being $0.63m$ at $E/\varepsilon_D = -1$, $0.95m$ at $E/\varepsilon_D = -2$, and $1.9m$, at $E/\varepsilon_D = -3$.

The effect of allowing nonadiabaticity in the electron-phonon interaction is to slightly increase the DOS and to shift the continuum-band edge. The DOS projected onto the phonon vacuum exhibits three distinct regimes when the coupling is sufficiently above the polaron threshold: (i) at shallow energies there is a shift of the continuum-band edge associated with the perturbative emission and reabsorption of virtual phonons, (ii) at intermediate energies there is linear exponential behavior of the DOS, where the electron finds a well and stabilizes it, and (iii) there is a deep tail region, extending to the polaron ground-state energy, where the electron has to dig its own potential well.

IV. COMBINED EFFECTS OF STATIC DISORDER AND ELECTRON-PHONON INTERACTION

The combined effects of static disorder in the form of a correlated Gaussian random potential and dynamic disorder due to zero-point motion of the lattice are now considered. Generalizing the physical argument of the previous section to this case, a static approximation to the band-tail DOS involves the quantum-mechanical probability distribution for Fourier components of the static potential and for normal coordinates q_k of the lattice at zero temperature:[21,22]

$$P\{V(k), q_{\text{k}}\} \propto \exp\left[-\frac{1}{2} \int \frac{d^3k}{(2\pi)^3} V(k) B^{-1}(k) V(-k) \right.$$
$$\left. - \sum_k \frac{M\omega_k}{\hbar} |q_{\text{k}}|^2 \right]. \qquad (4.1)$$

Here, the autocorrelation function is chosen to be

$$B(k) = V_{\text{rms}}^2 (\pi L^2)^{3/2} \exp\left[-\frac{k^2 L^2}{4} \right]. \qquad (4.2)$$

L is a measure of the spatial extent of the short-range order, and is typically of the order of the lattice spacing. Reference 25 discusses the effects of other choices of the autocorrelation function. We consider static potential wells of Gaussian form characterized by a depth V_0 and range A:

$$V(r) = -V_0 \exp\left[-\frac{r^2}{A^2} \right]. \qquad (4.3)$$

The forms of the quantum-mechanical zero-point lattice fluctuations and their autocorrelation function are

chosen to be precisely those described by Eqs. (3.3) and (3.4b), respectively.

The probability of occurrence of fluctuations (4.3) and (3.3) becomes

$$
\begin{aligned}
P\{V(k),q_k\} \propto \exp\Bigg[&- \frac{V_0^2}{2V_{rms}^2}\left[\frac{1}{Z}\right]^{3/2}(2-Z)^{-3/2} \\
&- \left[\frac{\pi}{bk_0}\right]^4 \frac{\hbar u k_0}{2\pi^3(\hbar^2/2MQ_0^2)} \\
&\times \left[1 - \frac{\pi}{(bk_0)^2}\right]^{-2}\Bigg] ,
\end{aligned} \quad (4.4)
$$

where $Z \equiv (L/A)^2$.

The constraint on the variational parameters Z, V_0, Q_0, and b is now expressed by the radial Schrödinger equation

$$
\begin{aligned}
\Bigg[&- \frac{\hbar^2}{2m}\frac{d^2}{dr^2} - V_0 e^{-r^2/A^2} + \frac{E_d}{u}\sum_k \dot{q}_k \frac{e^{i\mathbf{k}\cdot\mathbf{r}}}{\sqrt{N}} \\
&+ \frac{M}{2}\sum_k \omega_k^2 |q_k|^2 \Bigg] u(r) = -|E|u(r) ,
\end{aligned} \quad (4.5)
$$

which contains three potential terms: the static Gaussian potential, the deformation potential describing interaction between the electron and acoustic phonons, and the lattice distortion energy. As in the previous section, the variational parameters are chosen to maximize (4.4) subject to constraint (4.5).

For an appropriate choice of physical parameters, this method predicts linear exponential behavior of the DOS over the energy ranges of experimental interest, in close agreement with the path-integral predictions to be disussed next (Fig. 8). Over these energy regimes the extent of the localized state wave function is comparable to the correlation lengths arising from static disorder and phonons, namely the interatomic spacing.

To obtain the more general path-integral predictions which allow the incorporation of nonadiabaticity in the electron-phonon interaction, the term

$$
H_I = \sum_{j=1}^{N_d} v(\mathbf{x}-\mathbf{R}_j) \quad (4.6)
$$

is now added to the Hamiltonian (2.1), the sum being over N_d static impurity potentials located at $\{\mathbf{R}_j\}$. Following the methods of Edwards and Gulyaev[26] and Sumanthyakanit,[24] the contribution to the averaged Green's function is obtained by averaging over all configurations of the static potentials. The effective action (3.9) gains the term

$$
-i\hbar\rho \int d\mathbf{R}\left[\exp\left[-\frac{i}{\hbar}\int_0^t d\tau\, v[\mathbf{x}(\tau)-\mathbf{R}]\right]-1\right] , \quad (4.7)
$$

where $\rho \equiv N_d/V$ is the impurity density. In the limits of high density $(\rho \to \infty)$ and weak scattering $(v \to 0)$ where ρv^2 remains constant, (4.7) is simplified to

$$
\frac{i}{2\hbar}\int_0^t d\tau \int_0^t d\tau'\, B(\mathbf{x}(\tau)-\mathbf{x}(\tau')) , \quad (4.8)
$$

where the autocorrelation function for the impurity potentials is

$$
B(\mathbf{x}(\tau)-\mathbf{x}(\tau')) \equiv \rho \int d\mathbf{R}\, v(\mathbf{x}(\tau)-\mathbf{R})v(\mathbf{x}(\tau')-\mathbf{R}) . \quad (4.9)
$$

Here, the mean potential has been chosen to be zero:

$$
\int d\mathbf{R}\, v(\mathbf{x}(\tau)-\mathbf{R}) = 0 . \quad (4.10)
$$

The impurity potentials are assumed to have a Gaussian form, thus it follows form (4.9) that the autocorrelation function is given by Eq. (4.2). As in the previous section, the Green's function is approximated by a first-cumulant expansion about the harmonic oscillator trial action (3.11). Through the inclusion of the static impurity potentials, expression (3.18) gains the factor $\exp[J_{dis}(t)]$ where

$$
\begin{aligned}
J_{dis} = -\int_0^t d\Delta(t-\Delta)\Bigg[&\frac{(k_0L)^3 V_{rms}^2}{8\hbar^2} \\
&\times \left[\frac{(k_0L)^2}{4} - \frac{i}{2}Q(\Delta;t)\right]^{-3/2}\Bigg] .
\end{aligned} \quad (4.11)
$$

An equivalent static disorder contribution may also be derived by introducing a frozen-in phonon distribution.

Figure 5 presents the path-integral predictions for the DOS with the electron interacting with both static disorder and acoustic phonons. The physical parameters are chosen to give behavior close to that of glassy As$_2$Se$_3$ studied recently by Monroe and Kastner.[27] For $S_{ac}=0$ the DOS is close to linear exponential for energies 0.3–0.8 eV into the band gap, and it drops by five decades over this energy interval. V_{rms} is expected to be of the order of 1 eV.[24] The introduction of electron-phonon coupling leads to a slight increase in the projected density of states. At coupling to phonons just above polaron threshold $(S_{ac}=400)$, as is observed in some materials,[28] this increase in the DOS becomes quite notice-
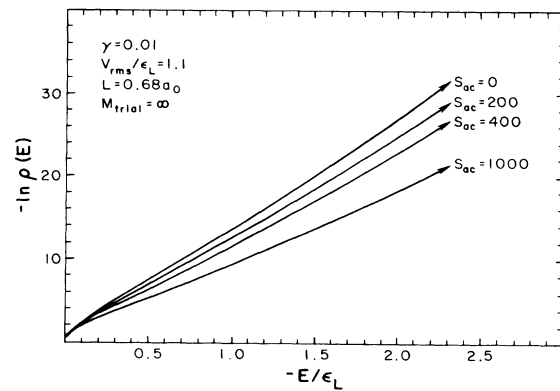

FIG. 5. Band-tail DOS with the combined effects of static disorder and electron-phonon interaction evaluated using the path integral. The mean static potential-well depth is fixed at $V_{rms}/\varepsilon_L = 1.1$ and the effects of increasingly strong coupling to phonons is presented. The energy unit is $\varepsilon_L \equiv \hbar^2/2mL^2$.

able. The high degree of linearity of the exponential band tail, however, is accurately preserved.

Note that in Fig. 5, for $S_{ac} = 200$, $S_{ac}\gamma$ is below threshold for small-polaron formation yet the DOS is still increased by allowing the electron to interact with phonons. This is a consequence of the static potential fluctuations acting as nucleation centers for small polaron formation. This synergetic interplay between static disorder and lattice dynamics is considerably more pronounced in the case of weak randomness.

Figure 6 presents the DOS for fixed coupling to phonons and increasingly strong static disorder. For no static disorder, the DOS goes to zero at the small-polaron ground-state energy. With the addition of weak static disorder the DOS extends to arbitrarily negative energies. This is because static potential fluctuations can support a bound state at an arbitrarily negative energy, although deeper fluctuations become more improbable. As the strength of the static disorder increases the DOS regains linear exponential behavior. In Fig. 7, it is apparent that for weak disorder the enhancement in the DOS is quite pronounced even for $S_{ac}\gamma$ considerably below small-polaron threshold.

Figures 5–7 are obtained in the infinite-effective-mass approximation. The effect of a variational trial mass is depicted in Fig. 8, where a comparison with the predictions of the physical argument is also made. The physical argument provides a more general static theory of the band-tail DOS than the path-integral method in the infinite-effective-mass approximation since in the former method the wave function is general whereas in the latter method it is restricted to a harmonic oscillator form. Thus the physical argument predicts a slightly greater DOS in the band tail. The path-integral method, however, does allow for the incorporation of nonadiabaticity which is absent in the static theory. This results in an overall increase of the DOS as compared with the predictions of the static path-integral method.

FIG. 7. Band tail DOS as in Fig. 5, but with the choice of a small mean potential-well depth $V_{rms}/\varepsilon_L = 0.50$. The electron-phonon coupling is below threshold for small-polaron formation in the absence of static disorder. The static potential wells act as small-polaron nucleation centers, breaking the energy barrier which prevents their formation when S_{ac} is small. Here, the synergetic effect is greater than in Fig. 5.

For large positive energies the DOS attains its square-root continuum behavior $\rho(E) \sim \sqrt{E}$. The continuum-band edge is shifted to a small negative energy as a consequence of a self-energy correction to the electron. Allowing for nonadiabaticity in the electron-phonon interaction results in a shift included in E_{GL} associated with the emission and reabsorption of virtual phonons. The shift due to weak static disorder is estimated[25] to be $-V_{rms}^2/2\varepsilon_L$. The finite-effective-mass result depicted in Fig. 8 reveals a relatively large shift in the continuum edge arising from a combination of static disorder and virtual phonons.

V. DISCUSSION

In summary, the band-tail DOS was calculated using a first-principles method for an electron interacting with
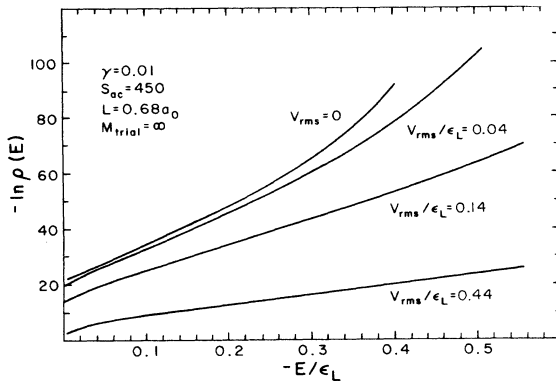

FIG. 6. Band-tail DOS with the combined effects of static disorder and electron-phonon interaction evaluated using the path integral. The coupling constant is fixed at $S_{ac} = 450$, just above threshold for small-polaron formation. In the absence of static disorder, the small-polaron ground-state energy is $E_{GS}/\varepsilon_L \approx -0.42$. The effects of increasing mean static potential-well depths is presented. The three curves with nonzero V_{rms} extend to arbitrarily negative energies.
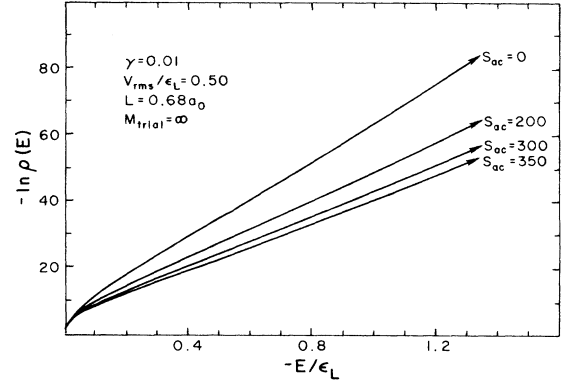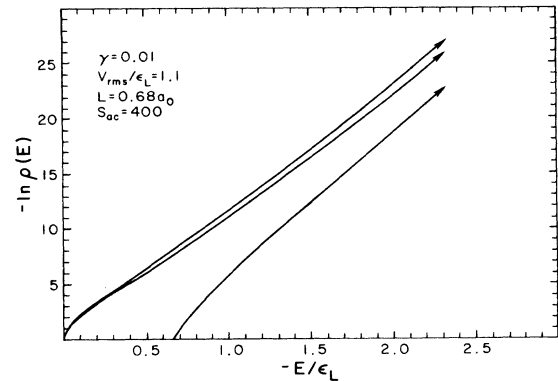

FIG. 8. Band-tail DOS for fixed S_{ac} and fixed V_{rms}, depicting three successively less restrictive solution methods. The top curve is the path-integral result in the infinite-effective-mass approximation; the middle curve is the prediction of the physical argument; and the bottom curve is the path-integral result with the variational trial mass chosen to maximize $\ln\rho(E)$. The shifted continuum-band edge is located at $E_B/\varepsilon_L \approx -V_{rms}^2/2\varepsilon_L^2 + E_{GL}/\varepsilon_L \approx -0.7$.

both static disorder, in the form of a correlated Gaussian random potential, and dynamic disorder, in the form of zero-point vibrations of the lattice. For a physically reasonable choice of physical parameters, this method predicts linear exponential behavior of the DOS over energy ranges of experimental interest.

The failure of previous first-principles approaches[1-4] to account for a broad range of linear exponential behavior in the band tail has sparked considerable effort to incorporate additional physical effects not contained in the original models of localization by a static Gaussian random potential. The most notable of these are excitonic effects[8,9] and the influence of finite temperature.[10] These studies have relied heavily on heuristic arguments. The methods we have employed in this paper will, hopefully, provide a first-principles framework from which to study these phenomena and in which the universality of linear exponential band tails is already apparent. More recently,[11,12] the use of Gaussian statistics for potential fluctuations has been called into question. Chan, Louie, and Phillips[11] have argued that in certain glasses that the probability distribution of potential fluctuations is itself a linear exponential in the depth of the potential well. This is fundamentally different from our approach, in which we retain Gaussian statistics for potential fluctuations as suggested by the central limit theorem. We believe that the universally observed exponential band tails in disordered materials can be explained by the proper inclusion of the effects of short-range order as described by the autocorrelation function (4.2) rather than by calling into question the applicability of the central limit theorem. Recently, this hypothesis has been examined by means of a detailed study[25] of the influence of the shape of the autocorrelation function on the extent and accuracy of linear exponential behavior of the band tail. This hypothesis may be tested experimentally by varying the spatial correlations in the randomness either by the addition of impurities or by varying the conditions under which the materials are prepared. Such variations may be shown to have a direct and predictable[25] influence on energy dependence of the one-electron density of states.

The continuum effective-mass model used here is accurate for band-tail states where the spatial extent of the localized state wave function is greater than or comparable to the lattice spacing. This condition is satisfied throughout most of the Urbach tail.

The high degree of linearity of the exponential band tail arising from static disorder alone is preserved even after the introduction of lattice dynamics. These results provide additional insight into the universality of Urbach tails in disordered solids as measured in optical absorption experiments. The actual magnitude of the density of states, however, may be enhanced considerably due to the interplay between disorder and the polaron tendency. This is particularly evident for relatively weak static disorder and electron–acoustic-phonon coupling just below polaron threshold. Such an enhancement of the effective electron-phonon coupling arising from disorder may play an important role in describing bipolaron formation in disordered systems and the nature of mobility edges in amorphous semiconductors.[29] It may

also be important for a complete description of superconduction instabilities in dirty materials.

APPENDIX: VARIATIONAL PRINCIPLE FOR THE BAND-TAIL DOS IN THE SADDLE-POINT APPROXIMATION

Define a function $G(t)$ so that the DOS has the form

$$\rho(E) \equiv \frac{1}{2\pi\hbar} \int dt \, \exp G(t) \ . \tag{A1}$$

What is considered here is the case where this time contour integral is dominated by a saddle point on the imaginary time axis: $t = -iT_0$. Then

$$2\pi\hbar\rho(E) \approx e^{G(-iT_0)} \left[\frac{\pi}{|G''(-iT_0)|} \right]^{1/2} . \tag{A2}$$

It follows from (3.7) and (3.10) that

$$e^{G(-iT_0)} = e^{ET_0/\hbar} \langle \mathbf{x} | e^{-H_{\text{eff}}T_0/\hbar} | \mathbf{x} \rangle \ , \tag{A3}$$

where H_{eff} is obtained from (2.1) through a trace over all phonon coordinates. For energies E less than zero, (A3) has a Feynman path-integral representation

$$e^{G(-iT_0)} = e^{-|E|T_0/\hbar} \int D\mathbf{x}(\tau) e^{-S_{\text{eff}}/\hbar}, \quad \mathbf{x}(0) = \mathbf{x}(T_0) = 0 \tag{A4}$$

where S_{eff} is real. The convexity of the exponential for real values of its argument then implies

$$e^{G(-iT_0)} \geq e^{-|E|T_0/\hbar} \left[\int D\mathbf{x}(\tau) e^{-S_{\text{trial}}/\hbar} \right] \\ \times e^{-\langle S_{\text{eff}} - S_{\text{trial}} \rangle /\hbar}, \tag{A5}$$

where the angular brackets are as in (3.15).

Consider the function

$$F(T_0) \equiv -\frac{|E|T_0}{\hbar} - \frac{1}{\hbar} \langle S_{\text{eff}} - S_{\text{trial}} \rangle \ . \tag{A6}$$

For real positive T_0, $F(T_0)$ has a local minimum when $T_0 = T_s$, thus

$$e^{F(T_0)} \geq e^{F(T_s)} \ . \tag{A7}$$

It follows that

$$2\pi\hbar\rho(E) \geq \left[\frac{\pi}{|G''(-iT_0)|} \right]^{1/2} \\ \times \left[\int D\mathbf{x}(\tau) e^{-S_{\text{trial}}/\hbar} \right] e^{F(T_s)} . \tag{A8}$$

Thus the greatest lower bound to the true DOS is obtained by maximizing $F(T_s)$ with respect to the variational parameters of the trial action.

[1]I. M. Lifshitz, Zh. Eksp. Teor. Fiz. **44**, 2100 (1963) [Sov. Phys.—JETP **17**, 1159 (1963)].

[2]E. O Kane, Phys. Rev. **131**, 79 (1963).

[3]B. I. Halperin and M. Lax, Phys. Rev. **148**, 722 (1966).

[4]J. L. Cardy, J. Phys. C **11**, L321 (1978).

[5]S. John and M. J. Stephen, J. Phys. C **17**, L559 (1984).

[6]W. Sritakool, V. Sayakanit, and H. R. Glyde, Phys. Rev. B **33**, 1199 (1986).

[7]S. John, C. Soukoulis, M. H. Cohen, and E. Economou, Phys. Rev. Lett. **57**, 1777 (1986).

[8]H. Sumi and Y. Toyozawa, J. Phys. Soc. Jpn. **31**, 342 (1971).

[9]J. Dow and D. Redfield, Phys. Rev. B **5**, 594 (1972).

[10]T. Skettrup, Phys. Rev. B **18**, 2622 (1978).

[11]C. T. Chan, S. G. Louie, and J. C. Phillips, Phys. Rev. B **35**, 2744 (1987).

[12]Y. Bar-Yam, D. Adler, and J. D. Joannopoulos, Phys. Rev. Lett. **57**, 467 (1986).

[13]P. W. Anderson, Phys. Rev. **109**, 1492 (1958).

[14]N. F. Mott, Adv. Phys. **16**, 49 (1967); Philos. Mag. **17**, 1259 (1968).

[15]E. Abrahams, P. W. Anderson, D. C. Licciardello, and T. V. Ramakrishnan, Phys. Rev. Lett. **42**, 673 (1979).

[16]L. Landau, Phys. Z. Sowjetunion **3**, 664 (1933).

[17]R. P. Feynman, Phys. Rev. **97**, 660 (1955); R. P. Feynman and A. R. Hibbs, *Quantum Mechanics and Path Integrals* (McGraw-Hill, New York, 1965).

[18]Y. Toyozawa, Prog. Theor. Phys. **26**, 29 (1961).

[19]A. Sumi and Y. Toyozawa, J. Phys. Soc. Jpn. **55**, 137 (1973).

[20]D. Emin and T. Holstein, Phys. Rev. Lett. **36**, 323 (1976).

[21]S. John and M. H. Cohen, Phys. Rev. B **34**, 2428 (1986).

[22]S. John, Phys. Rev. B **35**, 9291 (1987).

[23]F. Urbach, Phys. Rev. **92**, 1324 (1953); W. Martienssen, J. Phys. Chem. Solids **2**, 257 (1957).

[24]V. Samanthyakanit, J. Phys. C **7**, 2849 (1974).

[25]S. John, M. Chou, M. H. Cohen, and C. Soukoulis (unpublished).

[26]S. F. Edwards and Y. B. Gulyaev, Proc. Phys. Soc. London **83**, 495 (1964).

[27]D. Monroe and M. A. Kastner, Phys. Rev. B **33**, 8881 (1986).

[28]J. Bardeen and W. Shockley, Phys. Rev. **80**, 72 (1950).

[29]M. H. Cohen, E. N. Economou, and C. M. Soukoulis, Phys. Rev. Lett. **51**, 1202 (1983).